Deep Learning for Channel Estimation of 6G RIS-NOMA Systems with Hardware Impairments

Nhien Q. T. Thoong*, Adnan A. Cheema†, Saeed R. Khosravirad‡, Octavia A. Dobre*, Trung Q. Duong*
*Faculty of Engineering and Applied Science, Memorial University, St. John's, Canada.
†School of Engineering, Ulster University, Belfast, UK.
‡Nokia Bell Labs, Murray Hill, NJ, USA.
Emails: {qtnthoong, odobre, tduong}@mun.ca), a.cheema@ulster.ac.uk, saeed.khosravirad@nokia-bell-labs.com

***Abstract*—Reconfigurable intelligent surfaces (RIS) integrated with non-orthogonal multiple access (NOMA) are essential technologies for enhancing spectrum efficiency and coverage in sixth-generation (6G) wireless networks. Accurate channel estimation in RIS-NOMA systems is challenged by hardware impairments and user mobility, which introduce distortions and dynamic channel conditions. This paper proposes a hybrid convolutional neural network-long short-term memory (CNN-LSTM) model designed to improve channel estimation in RIS-NOMA environments affected by hardware impairments. The model leverages CNNs to extract spatial features from high-dimensional channel matrices and employs LSTMs to capture temporal variations resulting from user movement. Additionally, a dataset generation algorithm is developed to simulate time-varying RIS-NOMA scenarios with realistic hardware impairments. We evaluated the proposed model performance across various noise factors, demonstrating its capability to maintain accurate channel estimation under different hardware impairment levels and quantization bit settings, as measured by root mean squared error (RMSE), mean absolute error (MAE), and mean absolute percentage error (MAPE). Across different settings in RIS-NOMA systems, the proposed model achieved its best performance with an RMSE of 0.00186, MAE of 0.00148, and MAPE of 0.06501. Our findings highlight the model's adaptability and robustness, providing valuable insights for reliable channel estimation in complex RIS-NOMA systems.**

I. Introduction

Sixth-generation (6G) wireless technology represents the forthcoming evolution in communication networks with the potential to deliver transformative improvements in data rate, latency, connectivity and overall network performance [1]. Due to the surge in volumetric data, the proliferation of smart devices, and the emergence of sophisticated applications such as telemedicine [2], autonomous vehicles [3], and smart cities [4], there is an increasing demand for faster and more reliable networks. The development of 6G will be supported by several key technologies, including artificial intelligence (AI) [5] for network management and optimization, Terahertz (THz) [6] frequencies for faster communication and higher capacity, advanced multiple-input and multiple-output (MIMO) [7] systems for enhanced data throughput and network coverage, to name a few. However, a thorough exploration of these advanced technologies will be critical for addressing the associated challenges and managing the radio frequency electromagnetic field exposure levels [8].

One of such technology is reconfigurable intelligent surfaces (RIS), which have gained considerable attention for their ability to control wireless propagation environments. A RIS consists of a large array of passive or active reflecting elements which are capable of adjusting the phase and amplitude through programmable metasurfaces. By dynamically altering the propagation environment, RIS can enhance signal strength, extend coverage areas, and mitigate interference. This capability is particularly beneficial in environments with significant signal blockages, such as urban environments [9]. Moreover, RIS technology contributes to the energy efficiency of wireless networks by minimizing the need for high-power transmitters and reducing the overall energy consumption of communication systems [10]. Given these advantages, RIS is increasingly recognized as a key enabler for spectrum efficiency, coverage optimization, and energy efficiency in 6G.

Another emerging technology for 6G is non-orthogonal multiple access (NOMA), which offers an efficient approach to handling the massive connectivity demands of next-generation networks [11]. Unlike conventional orthogonal multiple access (OMA) techniques [12], [13], which allocate distinct time, frequency, or code resources to different users, NOMA allows multiple users to share the same frequency and time resources by superimposing their signals in the power domain. NOMA operates by allocating different power levels to users based on their channel conditions, allowing stronger users to subtract the interference from weaker users using successive interference cancellation (SIC). This allows multiple users to be served at the same time, enhancing both spectral efficiency and system throughput. The integration of RIS and NOMA provides a promising solution to key challenges in modern wireless communications [14]. By dynamically directing signals to target users, RIS reduces interference, enabling NOMA to more efficiently superimpose multiple user signals on shared resources. In addition, RIS overcomes signal blockages and expands coverage areas, allowing NOMA to serve users in areas with poor connectivity.

Despite the potential benefits brought by the combination of RIS and NOMA, the practical deployment of RIS-NOMA systems is affected by hardware impairments inherent in communication devices [14]–[16], such as phase noise, in-phase and quadrature (I/Q) imbalance, and nonlinearities in ampli-

fiers. These impairments introduce distortions and uncertainties into the transmitted and received signals, which reduces the accuracy of channel state information (CSI) estimation [16]. Moreover, the integration of RIS and NOMA substantially increases the complexity of the channel estimation process, as the large number of RIS elements and multiple users result in high-dimensional channel matrices. Hardware impairments further complicate this process by altering the propagation characteristics and introducing additional noise factors. Although previous studies have examined RIS-NOMA systems with hardware impairments [14], [17] and proposed various channel estimation techniques for RIS [18], [19], NOMA [20], [21], and RIS-NOMA systems [22], [23], research specifically addressing channel estimation in RIS-NOMA systems under hardware impairments remains limited. This gap limits their applicability and reliability in dynamic real-world environments.

This work proposes a deep learning model for channel estimation in practical RIS-NOMA systems affected by hardware impairments and user mobility. The proposed model leverages convolutional neural networks (CNNs) [24] to capture spatial features from high-dimensional channel matrices and integrates long short-term memory (LSTM) networks [25] to capture the temporal variations induced by user movement. By combining these architectures, the model effectively addresses the complexities of dynamic channel conditions and hardware-induced distortions. The main contributions of this paper are as follows and summarized in Table I:

- Development of a hybrid CNN-LSTM architecture for channel estimation in RIS-NOMA systems.
- Creation of a dataset generation algorithm that models time-varying RIS-NOMA environments with inherent hardware impairments.
- Execution of extensive simulations to evaluate and validate the proposed model's performance under varying hardware impairment factors.

TABLE I: Overview of prior research and this work.

Studies	RIS	NOMA	Hardware Impairments	Channel Estimation
[18], [19]	✓	×	×	✓
[20], [21]	×	✓	×	✓
[22], [23]	✓	✓	×	✓
[14], [17]	✓	✓	✓	×
This work	✓	✓	✓	✓

II. System Model and Problem Formulation

In this work, the considered downlink system comprises a single-antenna base station (BS), a RIS with N reflecting elements, and L single-antenna users (UEs) as shown in Fig. 1. The direct links between the BS and the UEs are assumed to be blocked due to the obstacles. Thus, the RIS assists the transmission between the BS and the UEs through the cascaded channel BS-RIS-UE$_l$, where $l \in \{1, 2, ..., L\}$. The UEs are assumed to gradually move away from the BS with a constant

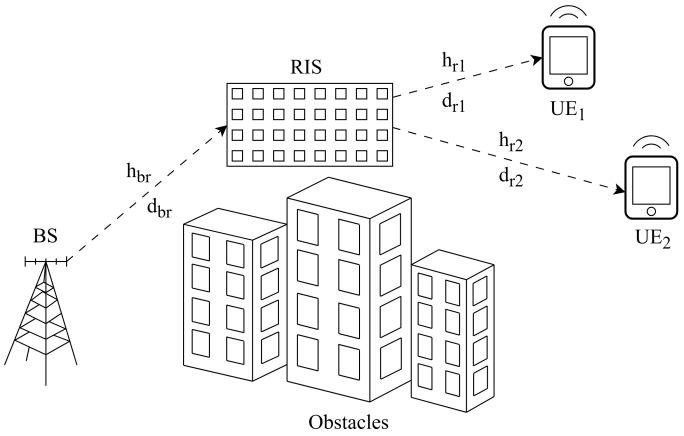

Fig. 1: A downlink RIS-NOMA wireless system.

speed v per time step t. The BS transmits a superimposed signal $x(t)$ as

$$x(t) = \sqrt{P_b}\left[a_1 x_1(t) + a_2 x_2(t) + ... + a_L x_L(t)\right], \quad (1)$$

where P_b is the BS transmission power, $x_l(t)$ denotes the signal for UE$_l$, and a_l represents the power allocation coefficient for each UE$_l$, which satisfies the relations $\sum_{l=1}^{L} a_l^2 = 1$ and $a_1 < a_2 < ... < a_L$. However, due to the non-ideal hardware at the BS, the superimposed signal is modelled as

$$\tilde{x}(t) = x(t) + \epsilon_b(t), \quad (2)$$

where $\epsilon_b \in \mathcal{CN}\left(0, \kappa_b^2 P_b\right)$ is the distortion noise caused by hardware impairments at the BS [26]. Here, κ_b is the constant that controls the level of impairment of the non-ideal hardware at the BS. The received signal at UE$_l$ at time t can be expressed as

$$y_l(t) = \sqrt{\Lambda_l(t)}\mathbf{h}_{rl}^{\dagger}(t)\mathbf{\Theta}(t)\mathbf{h}_{br}(t)\gamma\frac{\tilde{x}(t)}{\sqrt{P_b}} + \epsilon_{u_l}(t) + \eta_l(t), \quad (3)$$

where the path loss factor $\Lambda_l(t) = \Lambda_{rl}(t)\Lambda_{br}$, consists of $\Lambda_{rl}(t)$ which defines the path loss from the RIS to UE$_l$ and Λ_{br} represents the path loss from the BS to the RIS. Path loss is a distance-dependent parameter, given by $\Lambda(\widehat{d}) = (\widehat{d}/d_0)^{-\beta}$ where $\widehat{d}$ is the length of the link, d_0 is the reference distance, and β is the path loss exponent (PLE) of the link. The $\mathbf{h}_{rl}(t) \in \mathbb{C}^{N\times 1}$ and $\mathbf{h}_{br}(t) \in \mathbb{C}^{N\times 1}$ represent the channel matrices of the links RIS-to-UE$_l$ and BS-to-RIS, respectively. $\mathbf{H}_l(t)$ can be used to denote the cascaded BS-RIS-UE$_l$ channel $\sqrt{\Lambda_l(t)}\mathbf{h}_{rl}^{\dagger}(t)\mathbf{\Theta}(t)\mathbf{h}_{br}(t)$. The diagonal reflection coefficient matrix of RIS, denoted by $\mathbf{\Theta}(t)$, can be characterized as $\mathbf{\Theta}(t) = \left[\alpha_1 e^{j\tilde{\theta}_1(t)}, \alpha_2 e^{j\tilde{\theta}_2(t)}, ..., \alpha_N e^{j\tilde{\theta}_N(t)}\right]^T$, where α_n is the amplitude reflection coefficient and $\tilde{\theta}_n(t) \in [0, 2\pi]$ is the phase shift. Due to the RIS hardware impairments, the phase shift of the n-th reflecting element is modelled as

$$\tilde{\theta}_n(t) = \bar{\theta}_n(t) + \epsilon_{\theta_n}(t), \quad (4)$$

where $\bar{\theta}_n(t)$ represents the ideal phase shift, $\epsilon_{\theta_n}(t)$ is the phase noise of the n-th element. Hardware limitations of the RIS restrict the ideal phase shifts to a discrete set represented by 2^q (where $q \geq 1$), rather than allowing continuous phase shifts. The $\epsilon_{\theta_n}(t)$ is an identically and independently distributed

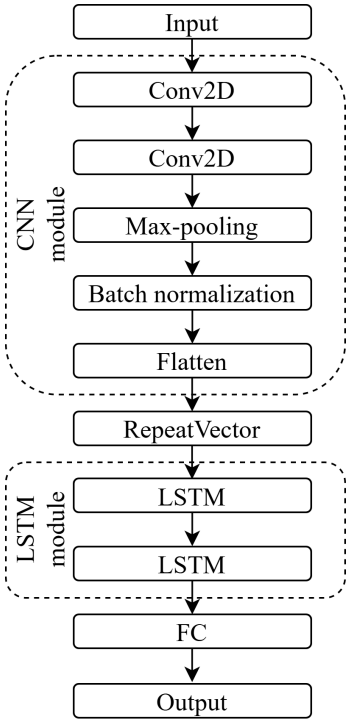

Fig. 2: CNN-LSTM model.

random variable and follows uniform distribution within the range $[-2^{-q}\pi, 2^{-q}\pi]$, where q is the number of quantization bits and characteristic function is given by $\phi_1 = \frac{\sin 2^{-q}\pi}{2^{-q}\pi}$ and $\phi_2 = \frac{\sin 2^{-q+1}\pi}{2^{-q+1}\pi}$. In equation (3), $\epsilon_{u_l}(t)$ indicates the distortion noise from hardware impairments at UE$_l$ and follows $\mathcal{CN}(0, \kappa_{u_l}^2 P_b |\sqrt{\Lambda_l(t)}\mathbf{h}_{rl}^{\dagger}(t)\boldsymbol{\Theta}(t)\mathbf{h}_{br}(t)|^2)$ [26], where κ_{u_l} is the constant that controls the level of impairment of the non-ideal hardware at UE$_l$. The $\eta_l(t)$ represents the complex additive white Gaussian noise (AWGN) with zero mean and variance σ^2 at UE$_l$. The transmit signal-to-noise ratio (SNR) is denoted by $\gamma = P_b/\sigma^2$.

This work focuses on the challenge of channel estimation in the considered RIS-NOMA scenario, where both time-varying channels and hardware impairments significantly impact system performance. In the considered system, the channel BS-to-RIS is assumed to be static, while the RIS-to-UE channels are slow time-varying due to user mobility at constant speed. This mobility results in dynamic channel conditions that evolve over each time step t. Furthermore, non-ideal hardware at the BS and UEs generates distortion noises while hardware limitations at the RIS cause phase noise in the reflection coefficients. These impairments degrade the quality of the transmitted and reflected signals, thereby introducing additional complexities to the channel estimation process and requiring further investigation.

III. Proposed Model

To address the challenge of channel estimation in the considered RIS-NOMA downlink scenario, a CNN-LSTM model is proposed. CNN is a powerful tool in machine learning thanks to its ability to process, analyze and identify complex patterns [24]. Recently, CNN has been found useful for time-series analysis and forecasting since they can capture local patterns and structures within temporal data. However, CNN may struggle with capturing long-term temporal dependencies effectively, a task that is more effectively addressed by LSTMs [25]. The LSTM networks are a special form of recurrent neural networks (RNNs) designed to address the challenges of learning long-term dependencies in sequential data [27]. Unlike RNNs, LSTMs are capable of retaining information over long periods thanks to their structured approach to updating and maintaining the cell state, which makes them particularly effective for tasks involving time and sequences. In the proposed model, CNN is used to identify spatial patterns in the input data. This process ensures the input data is well-structured for LSTM to effectively analyze and capture temporal dependencies. The architecture of the proposed CNN-LSTM model is presented in Fig. 2. Our proposed model captures local patterns in the input sequence using two two-dimensional convolutional (Conv2D) layers, each with 32 filters and a kernel size of 3. By applying "same" padding, the output retains the same length as the input sequence. To reduce computational complexity, a max-pooling layer is applied next, followed by a batch normalization layer, which helps stabilize and speed up training by reducing internal covariate shift. The model then reshapes the output from the previous layers into a one-dimensional (1D) vector using a flatten layer. This vector is passed through a RepeatVector layer, which replicates it to form a sequence suitable for processing by the LSTM layers. Each of the two stacked LSTM layers contains 32 hidden units, with the second layer added to refine the temporal dependencies learned by the model. Finally, a fully connected (FC) layer generates the model's output.

Algorithm 1: Dataset generation for RIS-NOMA scenarios.

Input: $N, P_b, a_1, a_2, \alpha_1, \alpha_2, \beta_1, \beta_2, d_0, d_{br}, d_{r1}, d_{r2}, \kappa_b, \kappa_{u_1}, \kappa_{u_2}, \gamma, v, T$.
Output: $\mathbf{Y}$ and $\mathbf{H}$.
Initialize empty arrays $\mathbf{Y}, \mathbf{H}, \mathbf{y}_t, \mathbf{H}_t$.
Initialize $L = 2$.
for $t = 1$ *to* T **do**
  Generate $x_1(t), x_2(t), \epsilon_b(t)$.
  Calculate $\tilde{x}(t)$ according to (2).
  Generate $\mathbf{h}_{br}(t)$, $\epsilon_{\theta_n}(t)$.
  for $l = 1$ *to* L **do**
    Generate $\mathbf{h}_{rl}(t)$, $\bar{\theta}_n^l(t)$, $\epsilon_{u_l}(t)$, $\eta_l(t)$.
    Calculate $\Lambda_l(t)$.
    Calculate $\tilde{\theta}_n^l(t)$ according to (4).
    Calculate $\boldsymbol{\Theta}_l(t)$.
    Calculate $y_l(t)$ according to (3).
    Calculate $\mathbf{H}_l(t)$.
    Calculate $d_{rl}(t) = d_{rl}(t) + v$.
    Append $y_l(t)$, $\mathbf{H}_l(t)$ to $\mathbf{y}_t$, $\mathbf{H}_t$ respectively.
  Append $\mathbf{y}_t$, $\mathbf{H}_t$ to $\mathbf{Y}$, $\mathbf{H}$ respectively.
return $\mathbf{Y}$ and $\mathbf{H}$.

IV. Simulations, Results and Discussions

This section outlines the simulation configuration and discusses the results obtained from channel estimation for the RIS-NOMA system with hardware impairments using the proposed CNN-LSTM model.

A. Simulation Configuration

According to Algorithm 1, a total of T samples are generated, with each sample representing a time step t in the RIS-NOMA system. The channel gains $\mathbf{h}_{rl}$ and $\mathbf{h}_{br}$, as well as the signal x_l at UE$_l$ are modelled as independent and following complex Gaussian distributions. The received signal at the UEs, denoted by $\mathbf{Y}$, and the cascaded channel BS-RIS-UE, denoted by $\mathbf{H}$, serve as the input and output, respectively, for the proposed model. Prior to feeding them to the model, data processing is performed. $\mathbf{Y}$ is represented as $\mathbf{Y} = [\mathbf{Y}(1), \mathbf{Y}(2), ..., \mathbf{Y}(T)]$, where each $\mathbf{Y}(t) = [y_1(t), y_2(t), ..., y_L(t)]$. Since each $y_l(t)$ is a complex value and cannot be directly fed into the DL model, the magnitude and phase of each $y_l(t)$ are calculated and concatenated to form a single dimension. The same transformation is applied to the cascaded channels BS-RIS-UE, denoted by $\mathbf{H} = [\mathbf{H}(1), \mathbf{H}(2), ..., \mathbf{H}(T)]$, where $\mathbf{H}(t) = [H_1(t), H_2(t), ..., H_L(t)]$. The magnitude of $\mathbf{H}$ is used as the output for the proposed model, while the magnitude and phase of $\mathbf{Y}$ serve as the input for training the model. The entire dataset of T samples for $\mathbf{Y}(t)$ and $\mathbf{H}(t)$ is then converted into time-series sequences with t_1 time steps, respectively. After this conversion, the length of the dataset becomes T'. The concept of 6G is still under development, and currently, no established standards exist for system-level parameters designed for specific use cases or scenarios. Hence, this paper proposes a possible parameter configuration for implementing a RIS-NOMA system model in 6G. In this paper, the reference distance d_0, the distance between the BS and the RIS d_{br}, the distance from the RIS to the first user d_{r1} and to the second user d_{r2} are respectively set to 20 m, 150 m, 30 m and 40 m. At each time step t, each UE$_l$ moves further away from the BS at a constant speed of 0.1 m per step. The PLE for both the BS-to-RIS and RIS-to-UE links is set to be 2.2. The RIS-NOMA system configuration is characterized by $\gamma = 20$ dB, $N = 20$, $a_1^2 = 0.3$, $\kappa_b = 0.1$. The $x_l(t)$ and $\mathbf{h}_{br}(t)$ are modelled as the distribution $\mathcal{CN} \sim (1, 0.1)$ while $\mathbf{h}_{r1}(t)$ and $\mathbf{h}_{r2}(t)$ follow $\mathcal{CN} \sim (4, 1)$ and $\mathcal{CN} \sim (3, 1)$, respectively. The amplitude reflection coefficient α_n is set to 1 and the phase shifts $\bar{\theta}_n$ are uniformly generated within the range $[0.01\pi, 0.02\pi]$. The performance of the proposed model is evaluated under various RIS-NOMA scenarios by varying hardware impairment factors $\kappa_{u_l} = \{0, 0.05, ..., 0.2\}$ and the number of quantization bits $q = \{1, 2, ..., 5\}$. A total of 8000 data points are used for training and testing. For each RIS-NOMA scenario, the dataset is normalized to the range $[0, 1]$ and divided, with 80% allocated for training and 20% reserved for testing. The dataset generation, model training and evaluation processes are implemented using the Python.

TABLE II: Performance of CNN-LSTM model with different number of time steps.

No. of time steps	RMSE	MAE	MAPE
10	0.00274	0.00221	0.10234
15	0.00244	0.00198	0.08907
20	**0.00206**	**0.00166**	**0.07374**
25	0.00232	0.00186	0.08317
30	0.00499	0.00454	0.20613

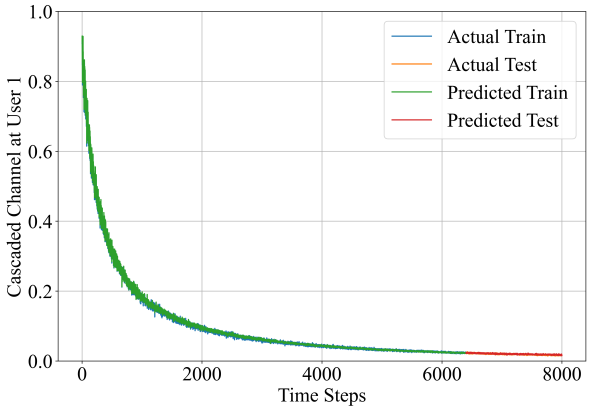

Fig. 3: Prediction performance on user 1.

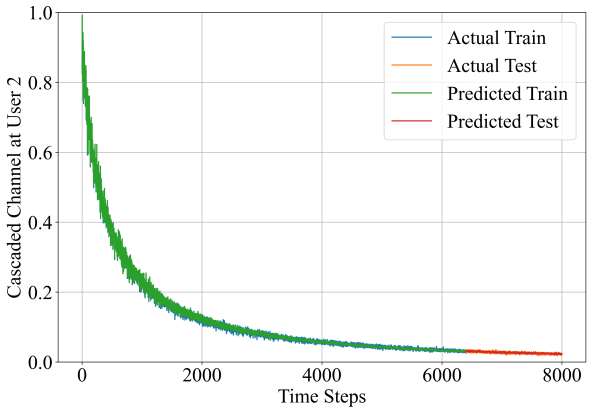

Fig. 4: Prediction performance on user 2.

B. Results and Discussion

Table II illustrates the performance of the proposed CNN-LSTM model for channel estimation in RIS-NOMA systems across varying numbers of time steps i.e., sequence length. For this scenario, the RIS-NOMA configuration is set with $\kappa_{u_l} = 0.1$ and $q = 3$. The model's effectiveness is evaluated using three key metrics: a) root mean squared error (RMSE), b) mean absolute error (MAE), and c) mean absolute percentage error (MAPE) on the test dataset. These metrics are chosen as they comprehensively assess the performance of channel estimation from different perspectives. RMSE is sensitive to large errors, making it suitable for identifying significant deviations. MAE is suitable for understanding general performance since

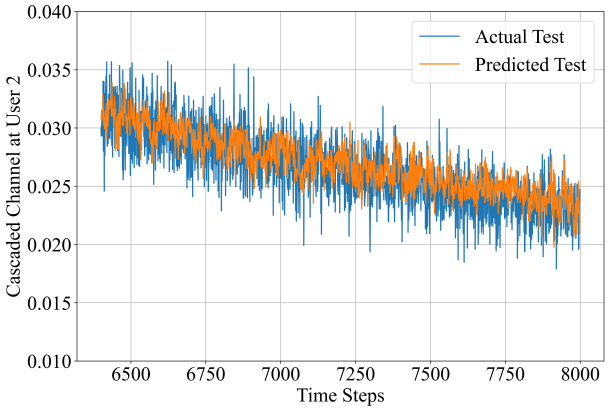

Fig. 5: Prediction performance on user 2 using test data.

it provides a straightforward measure of the average error. On the other hand, MAPE evaluates relative errors in percentage terms, which is particularly suitable for comparing performance across datasets with varying scales. For each metric, the average value is calculated as the mean of the results for user 1 and user 2. As presented in Table II, the proposed model demonstrates consistent performance across different sequence lengths. Specifically, RMSE, MAE, and MAPE values show variability with changes in the number of time steps. When the number of time steps is set to 20, the model achieves an improved accuracy compared to shorter sequences. When the number of time steps is increased beyond 20, as seen with 25 and 30 time steps, all RMSE, MAE, and MAPE metrics have poor performance. This trend suggests that while moderate sequence lengths contribute to enhanced performance, excessively long sequences may introduce complexities that affect estimation accuracy. Conversely, shorter sequences may not provide sufficient temporal context for the model to fully capture the underlying channel dynamics, leading to relatively higher errors. So, we are considering 20 time steps i.e., sequence length as an optimum value for the evaluation of all remaining RIS-NOMA scenarios in this work.

Fig. 3 and Fig. 4 show the prediction performance of the proposed model for user 1 and user 2, respectively, on both training and testing datasets over time steps. The system is configured with $\kappa_{u_l} = 0.1$ and $q = 3$. The results show that the model closely follows the actual channel values, indicating effective learning of the channel's temporal dynamics. For user 1, the model achieves an RMSE of 0.00168 on the test dataset, an MAE of 0.00136, and an MAPE of 0.07122. For user 2, the test set yields an RMSE of 0.00245, an MAE of 0.00196, and a MAPE of 0.07626. These metrics demonstrate that the model maintains a low prediction error across the test data, with minimal deviation from the actual values. Fig. 5 shows the prediction performance for user 2 on the test data. These figures demonstrate that the proposed model can adapt to both the overall trend and finer variations within the channel.

Table III presents the performance of the proposed CNN-LSTM model under varying levels of hardware impairment factors, with the number of quantization bits q fixed at 3. The proposed model demonstrates high accuracy in scenarios with minimal hardware impairments. At $\kappa_{u_l} = 0$, representing an ideal hardware condition with no impairments at the UEs, the model achieves an RMSE of 0.00195, an MAE of 0.00156, and a MAPE of 0.06688. Introducing slight hardware impairments ($\kappa_{u_l} = 0.05$ and $\kappa_{u_l} = 0.10$) results in minor increases in all RMSE, MAE, and MAPE. These small increments suggest that the proposed model maintains robust performance when minor hardware-induced distortions are present. However, as the hardware impairment factor continues to increase beyond $\kappa_{u_l} = 0.10$, RMSE, MAE, and MAPE show an upward trend. Nonetheless, the model continues to function effectively, adapting to more pronounced hardware imperfections. The observed performance variations underscore the model's ability to handle a range of hardware impairment scenarios. The slight increases in error metrics with higher impairment levels reflect the inherent challenges posed by more significant hardware imperfections, yet the model remains effective in adapting to these conditions.

TABLE III: Performance of CNN-LSTM model with different values of hardware impairment factors κ_{u_l}.

κ_{u_l}	**RMSE**	**MAE**	**MAPE**
0	0.00195	0.00156	0.06688
0.05	0.00196	0.00157	0.06885
0.10	0.00206	0.00166	0.07374
0.15	0.00316	0.00265	0.12072
0.2	0.00389	0.00336	0.15474

TABLE IV: Performance of CNN-LSTM model with a varying number of quantization bits q.

q	**RMSE**	**MAE**	**MAPE**
1	0.00524	0.00415	0.18688
2	0.00229	0.00183	0.07889
3	0.00206	0.00166	0.07374
4	0.00186	0.00148	0.06501
5	0.00195	0.00156	0.06921

Table IV presents the performance of the proposed CNN-LSTM model across different numbers of quantization bits q. The results indicate that the CNN-LSTM model consistently maintains low error rates across different q values, demonstrating its adaptability to varying phase adjustment resolutions. As the number of quantization bits increases from $q = 1$ to $q = 4$, all RMSE, MAE, and MAPE values generally decrease, indicating enhanced channel estimation accuracy with finer phase adjustments. This trend suggests that higher q values enable the model to capture more precise signal reflections and better represent the channel characteristics. At $q = 5$, a slight increase in RMSE, MAE, and MAPE is observed compared to $q = 4$. This variation may be attributed to the reduced phase noise in the system at a higher number of quantization bits. While lower phase noise typically enhances model accuracy by providing cleaner and more consistent training data, it also results in less variability within the channel patterns. Consequently, the CNN-LSTM model may become more specialized to the training

data, potentially limiting its ability to generalize effectively to unseen testing data. The slight performance variation at $q = 5$ highlights the importance of balancing phase resolution and model generalization to achieve optimal performance across diverse hardware configurations.

V. Conclusion

This paper presents a hybrid CNN-LSTM model for channel estimation in RIS-NOMA systems, effectively addressing the challenges posed by hardware impairments and user mobility. By integrating CNN architecture for spatial feature extraction and LSTM networks for modelling temporal dynamics, the proposed architecture enhances the accuracy of channel estimation in high-dimensional and dynamic environments. Simulation results indicate that the CNN-LSTM model maintains reliable performance under various conditions of hardware impairments. The model consistently achieves low RMSE, MAE, and MAPE, showcasing its robustness and adaptability in different RIS-NOMA configurations. Notably, the model effectively manages varying degrees of hardware-induced distortions, ensuring accurate channel estimation even under challenging conditions. Future research will explore advanced regularization techniques to enhance the model's generalization capabilities and mitigate overfitting. Additionally, investigating the impact of diverse noise types on channel estimation performance will provide deeper insights into optimizing the model for various operational conditions.

Acknowledgements

This work of N. Q. T. Thoong and T. Q. Duong was supported in part by the Canada Excellence Research Chair (CERC) Program CERC-2022-00109. The work of O. A. Dobre was supported in part by the Canada Research Chair Program CRC-2022-00187.

References

[1] Z. Zhang *et al.*, "Active RIS vs. passive RIS: Which will prevail in 6G?" *IEEE Trans. Commun.*, vol. 71, no. 3, pp. 1707–1725, Mar. 2023.

[2] S. T. Ahmed *et al.*, "6GTelMED: Resources recommendation framework on 6G enabled distributed telemedicine using edge-AI," *IEEE Trans. Consum. Electron.*, vol. 70, no. 3, pp. 5524–5532, Aug. 2024.

[3] S. Jain *et al.*, "Blockchain and autonomous vehicles: Recent advances and future directions," *IEEE Access*, vol. 9, pp. 130 264–130 328, Sep. 2021.

[4] N. Parvaresh and B. Kantarci, "A continuous actor-critic deep Q-learning-enabled deployment of UAV base stations: Toward 6G small cells in the skies of smart cities," *IEEE Open J. Commun. Soc.*, vol. 4, pp. 700–712, Mar. 2023.

[5] K. B. Letaief, Y. Shi, J. Lu, and J. Lu, "Edge artificial intelligence for 6G: Vision, enabling technologies, and applications," *IEEE J. Sel. Areas Commun.*, vol. 40, no. 1, pp. 5–36, Jan. 2022.

[6] I. F. Akyildiz, C. Han, Z. Hu, S. Nie, and J. M. Jornet, "Terahertz band communication: An old problem revisited and research directions for the next decade," *IEEE Trans. Commun.*, vol. 70, no. 6, pp. 4250–4285, Jun. 2022.

[7] Z. Wan, Z. Gao, F. Gao, M. D. Renzo, and M.-S. Alouini, "Terahertz massive MIMO with holographic reconfigurable intelligent surfaces," *IEEE Trans. Commun.*, vol. 69, no. 7, pp. 4732–4750, 2021.

[8] C. Nguyen *et al.*, "Deep learning models for time-series forecasting of RF-EMF in wireless networks," *IEEE Open J. Commun. Soc.*, vol. 5, pp. 1399–1414, 2024.

[9] X. Fan *et al.*, "RIS-assisted UAV for fresh data collection in 3D urban environments: A deep reinforcement learning approach," *IEEE Trans. Veh. Technol.*, vol. 72, no. 1, pp. 632–647, Jan. 2023.

[10] L. You *et al.*, "Energy efficiency and spectral efficiency tradeoff in RIS-aided multiuser MIMO uplink transmission," *IEEE Trans. Signal Process.*, vol. 69, pp. 1407–1421, 2021.

[11] Y. Liu *et al.*, "Evolution of NOMA toward next generation multiple access (NGMA) for 6G," *IEEE J. Sel. Areas Commun.*, vol. 40, no. 4, pp. 1037–1071, Apr. 2022.

[12] Y. Cheng, K. H. Li, Y. Liu, K. C. Teh, and H. V. Poor, "Downlink and uplink intelligent reflecting surface aided networks: NOMA and OMA," *IEEE Trans. Wirel. Commun.*, vol. 20, no. 6, pp. 3988–4000, Jun. 2021.

[13] B. Zheng, Q. Wu, and R. Zhang, "Intelligent reflecting surface-assisted multiple access with user pairing: NOMA or OMA?" *IEEE Commun. Lett.*, vol. 24, no. 4, pp. 753–757, Apr. 2020.

[14] X. Yue *et al.*, "Exploiting active RIS in NOMA networks with hardware impairments," *IEEE Trans. Veh. Technol.*, vol. 73, no. 6, pp. 8207–8221, Jun. 2024.

[15] M.-A. Badiu and J. P. Coon, "Communication through a large reflecting surface with phase errors," *IEEE Wirel. Commun. Lett.*, vol. 9, no. 2, pp. 184–188, Feb. 2020.

[16] J. Dai, F. Zhu, C. Pan, H. Ren, and K. Wang, "Statistical CSI-based transmission design for reconfigurable intelligent surface-aided massive MIMO systems with hardware impairments," *IEEE Wirel. Commun. Lett.*, vol. 11, no. 1, pp. 38–42, Jan. 2022.

[17] M. H. N. Shaikh, V. A. Bohara, A. Srivastava, and G. Ghatak, "A downlink RIS-aided NOMA system with hardware impairments: Performance characterization and analysis," *IEEE Open J. Signal Process.*, vol. 3, pp. 288–305, Jul. 2022.

[18] H. Feng, Y. Xu, and Y. Zhao, "Deep learning-based joint channel estimation and CSI feedback for RIS-assisted communications," *IEEE Commun. Lett.*, vol. 28, no. 8, pp. 1860–1864, Aug. 2024.

[19] H. Li, P. Zhiwen, W. Bin, L. Nan, and Y. Xiaohu, "Channel estimation for reconfigurable-intelligent-surface-aided multiuser communication systems exploiting statistical CSI of correlated RIS–user channels," *IEEE Internet Things J.*, vol. 11, no. 5, pp. 8871–8881, Mar. 2024.

[20] A. Salari, M. Shirvanimoghaddam, M. B. Shahab, Y. Li, and S. Johnson, "NOMA joint channel estimation and signal detection using rotational invariant codes and GMM-based clustering," *IEEE Commun. Lett.*, vol. 26, no. 10, pp. 2485–2489, Oct. 2022.

[21] M. H. Rahman, M. A. S. Sejan, M. A. Aziz, Y.-H. You, and H.-K. Song, "HyDNN: A hybrid deep learning framework based multiuser uplink channel estimation and signal detection for NOMA-OFDM system," *IEEE Access*, vol. 11, pp. 66 742–66 755, 2023.

[22] N. Q. T. Thoong, A. A. Cheema, S. R. Khosravirad, O. A. Dobre, and T. Q. Duong, "Channel estimation for reconfigurable intelligent surface-aided 6G NOMA systems using CNN-based quantum LSTM model," in *2024 IEEE 100th Veh. Technol. Conf. (VTC2024-Fall)*, Washington DC, USA, Oct. 2024.

[23] C. Nguyen, T. M. Hoang, and A. A. Cheema, "Channel estimation using CNN-LSTM in RIS-NOMA assisted 6G network," *IEEE Trans. Mach. Learn. Commun. Netw.*, vol. 1, pp. 43–60, May 2023.

[24] Z. Li, F. Liu, W. Yang, S. Peng, and J. Zhou, "A survey of convolutional neural networks: Analysis, applications, and prospects," *IEEE Trans. Neural Netw. Learn. Syst.*, vol. 33, no. 12, pp. 6999–7019, Dec. 2022.

[25] K. Greff, R. K. Srivastava., J. Koutník, B. R. Steunebrink, and J. Schmidhuber, "LSTM: A search space odyssey," *IEEE Trans. Neural Netw. Learn. Syst.*, vol. 28, no. 10, pp. 2222–2232, Oct. 2017.

[26] E. Björnson, M. Matthaiou, and M. Debbah, "A new look at dual-hop relaying: Performance limits with hardware impairments," *IEEE Trans. Commun.*, vol. 61, no. 11, pp. 4512–4525, Nov. 2013.

[27] W. Kong *et al.*, "Short-term residential load forecasting based on LSTM recurrent neural network," *IEEE Trans. Smart Grid*, vol. 10, no. 1, pp. 841–851, Jan. 2019.